Biomaterials 35 (2014) 9517–9528

Contents lists available at ScienceDirect

Biomaterials

journal homepage: www.elsevier.com/locate/biomaterials

The relationship between the diameter of chemically-functionalized multi-walled carbon nanotubes and their organ biodistribution profiles *in vivo*

Julie T-W. Wang [a, b, 1], Chiara Fabbro [c, d, 1], Enrica Venturelli [e, 1], Cécilia Ménard-Moyon [e], Olivier Chaloin [e], Tatiana Da Ros [c], Laura Methven [a], Antonio Nunes [a], Jane K. Sosabowski [f], Stephen J. Mather [f], Martyn K. Robinson [g], Julien Amadou [h], Maurizio Prato [c, ****], Alberto Bianco [d, ***], Kostas Kostarelos [a, **], Khuloud T. Al-Jamal [a, b, *]

[a] *Nanomedicine Laboratory, Centre for Drug Delivery Research, UCL-School of Pharmacy, University College London, London WC1N 1AX, UK*
[b] *Institute of Pharmaceutical Science, King's College London, London SE1 9NH, UK*
[c] *Dipartimento di Scienze Chimiche e Farmaceutiche, Università di Trieste, Trieste 34127, Italy*
[d] *Dipartimento di Scienze Molecolari e Nanosistemi, Università Ca'Foscari di Venezia, Venezia 30123, Italy*
[e] *CNRS, Institut de Biologie Moléculaire et Cellulaire, Laboratoire d'Immunopathologie et Chimie Thérapeutique, Strasbourg F-67000, France*
[f] *Centre for Molecular Oncology, Barts Cancer Institute, Queen Mary University of London, London EC1M 6BQ, UK*
[g] *UCB Celltech, Slough, Berkshire SL1 3WE, UK*
[h] *Nanocyl SA, Sambreville B-5060, Belgium*

ARTICLE INFO

Article history:
Received 16 May 2014
Accepted 25 July 2014
Available online 29 August 2014

Keywords:
Carbon nanotubes
Functionalization
SPECT/CT
Organ biodistribution

ABSTRACT

Carbon nanotubes (CNTs) exhibit unique properties which have led to their applications in the biomedical field as novel delivery systems for diagnosis and therapy purposes. We have previously reported that the degree of functionalization of CNTs is a key factor determining their biological behaviour. The present study broadens the spectrum by investigating the impact of the diameter of CNTs using two series of multi-walled CNTs (MWNTs) with distinct differences in their diameters. Both MWNTs were doubly functionalized by 1,3-dipolar cycloaddition and amidation reactions, allowing the appended functional groups to be further conjugated with radionuclide chelating moieties and antibodies or antibody fragments. All constructs possessed comparable degree of functionalization and were characterized by thermogravimetric analysis, transmission electron microscopy, gel electrophoresis and surface plasmon resonance. The MWNT conjugates were radio-labelled with indium-111, which thereby enabled *in vivo* single photon emission computed tomography/computed tomography (SPECT/CT) imaging and organ biodistribution study using γ-scintigraphy. The narrow MWNTs (average diameter: 9.2 nm) demonstrated enhanced tissue affinity including non-reticular endothelial tissues compared to the wider MWNTs (average diameter: 39.5 nm). The results indicate that the higher aspect ratio of narrow MWNTs may be beneficial for their future biological applications due to higher tissue accumulation.

* Corresponding author. Institute of Pharmaceutical Science, King's College London, Franklin-Wilkins Building, 150 Stamford Street, London SE1 9NH, UK.
** Corresponding author. Current address: Nanomedicine Lab, School of Medicine & National Graphene Institute, The University of Manchester, AV Hill Building, Manchester M13 9PT, UK.
*** Corresponding author. CNRS, Institut de Biologie Moléculaire et Cellulaire, Laboratoire d'Immunopathologie et Chimie Thérapeutique, UPR 3572, Strasbourg, 67000, France.
**** Corresponding author. Center of Excellence for Nanostructured Materials (CENMAT), INSTM, Unit of Trieste, Dipartimento di Scienze Chimiche e Farmaceutiche, Università di Trieste, Piazzale Europa 1, Trieste 34127, Italy.
E-mail addresses: prato@units.it (M. Prato), a.bianco@ibmc-cnrs.unistra.fr (A. Bianco), kostas.kostarelos@manchester.ac.uk (K. Kostarelos), khuloud.al-jamal@kcl.ac.uk (K.T. Al-Jamal).
[1] These authors contributed equally to this work.

http://dx.doi.org/10.1016/j.biomaterials.2014.07.054
0142-9612/

1. Introduction

Carbon nanotubes (CNTs) are needle-like nano-constructs composed of rolled-up graphene sheets made up of solely carbon atoms [1]. CNTs are famed for the unique electrical, mechanical and chemical properties leading to enormous applications in many fields including nanotechnology, electronics, and composite material science [2–5]. Over the past decades, developments in their surface functionalization strategies were successful in converting the water-insoluble pristine CNTs into biocompatible materials which are highly needed for drug delivery applications [6–8]. One of the most common approaches in CNT functionalization was developed by Prato and co-workers [9] in which a 1,3-dipolar cycloaddition reaction was carried out to introduce hydrophilic pendant groups onto the CNT sidewall [10]. This approach allowed mono- or multi-functionalization of the CNTs with biological molecules such as peptides and proteins to be potentially used for specific biomedical purposes [7].

For the development of drug delivery vehicles, it is important to investigate how the materials interact with biological barriers and distribute into different compartments of the body after systemic administration. Up to date, many studies have been carried out to investigate the biological behaviour of functionalized CNT (*f*-CNT) *in vitro* and *in vivo*. Results so far have indicated that both single-walled carbon nanotubes (SWNTs) and multi-walled carbon nanotubes (MWNTs) show signs of biocompatibility after adequate surface functionalization and upon shortening in contrast to their pristine counterparts [11–14]. It should also be noted that many of the adverse effects related to CNTs *in vivo* were reported for relatively long CNTs, either pristine or functionalized [15,16].

In vivo studies on organ biodistribution profiling of different types of *f*-CNTs have been documented. For instance, it was reported that short or individualized CNTs can undergo fast renal excretion, resulting in less tissue accumulation [17–19] while CNT coated with polyethyleneglycol (PEG) prolonged their blood circulation time and expanded their biomedical applications as drug delivery carriers [20]. Furthermore, conjugation with specific ligands was able to enhance uptake in tumours [21,22] and other organs [23]. Nevertheless, the effect of functionalized MWNT (*f*-MWNT) diameter on their organ biodistribution has not been studied before as previous studies by others have focused on the diameter as a determining factor in inducing lung toxicity [24,25].

The current study compares the organ biodistribution profiles of two types of chemically functionalized MWNTs with distinct differences in their diameter (mean values 39.5 nm *vs* 9.2 nm) using the quantitative γ-scintigraphy and SPECT/CT imaging. Initially, wide multi-walled nanotubes (*W*-MWNTs) and narrow multi-walled nanotubes (*N*-MWNTs) were shortened by an oxidative treatment so that similar length distributions (200–400 nm) were obtained. The MWNTs were then doubly functionalized by 1,3-dipolar cycloaddition and amidation reactions [26]. Further modifications were performed by covalent linking to a model humanized IgG antibody or its fragment antigen binding region (Fab′) against polymorphic epithelial mucin (MUC1) for possible future applications in targeted cancer therapeutics delivery. Both IgG and Fab′ have targeting capabilities, but their different size could possibly affect the biodistribution of the conjugates. All constructs were also derivatized with diethylenetriaminepentaacetic (DTPA) dianhydride chelating molecules for subsequent complexation of the nuclear imaging probe indium-111. This comparative study was designed to assess how the diameter of *f*-CNTs of various surface derivatization could impact their organ biodistribution *in vivo*.

2. Materials and methods

2.1. Materials

Chemicals were purchased from Sigma–Aldrich or Acros Organics and used as received. The *W*-MWNTs were purchased from Nanostructured & Amorphous Materials (stock# 1240XH) and the *N*-MWNTs were obtained from Nanocyl (batch# 171119). Both MWNTs were produced by the catalytic carbon vapour deposition process with 95+ % purity. Antibody hCTM01 IgG and Fab′ against polymorphic epithelial mucin (MUC1) were obtained from UCB Celltech.

2.2. Preparation of the thiolated IgG and Fab′ derivatives

IgG solution was prepared in PBS (5 mM EDTA, 50 mM $NaHCO_3$, pH 7.8) at the concentration of 67 μM. A freshly prepared solution of 2-iminothiolane·HCl (2-IT, Traut's reagent) (90 μL, 14.5 mM) in the same buffer was added to 1 mL of antibody solution to reach a final 2-IT concentration of 1.3 mM, corresponding to approximately 20 equivalents with respect to the IgG. The mixture was shaken for 1 h at room temperature (RT), followed by dialysis (Regenerated cellulose membrane, molecular weight cut-off (MWCO) = 12–14 kDa, Spectrum Laboratories) against PBS (5 mM EDTA, pH 6.5) at 4 °C to remove excess 2-IT.

In case of Fab′ samples, a Fab′ solution (1.8 mL, 123 μM) in 50 mM sodium acetate (2 mM EDTA, pH 5.6) was mixed with a freshly prepared 2-mercaptoethylamine solution (36 μL, 200 mM) in the same buffer to reach a final 2-mercaptoethylamine concentration of 4 mM, corresponding to approximately 32 equivalents with respect to Fab′. The mixture was shaken for 2 h at RT and purified by size exclusion chromatography using PD-10 desalting columns pre-packed with Sephadex G-25 Medium, equipped with a LabMate PD-10 Buffer Reservoir (GE Healthcare).

2.3. Chemical functionalization of MWNTs and substitution with IgG and Fab′

N-Pht-amino-diethoxy-ethyl amine and *N*-Boc-amino-diethoxy-ethylamino-acetic acid were prepared as previously described [26].

When anhydrous reaction conditions were required, reaction flasks were dried with a heating gun (300–500 °C), placed under high vacuum using a Schlenk line and purged with Ar. To keep the atmosphere dry and inert, balloons filled with Ar were used.

CNT washing procedure by filtration consisted of dispersing the nanotubes in the specified solvent (at a concentration of about 1 mg/mL), followed by sonication for 15–20 min and vacuum filtration on polytetrafluoroethylene (PTFE) Millipore filters (pore size: 0.1 μm). The procedure was repeated twice or three times for each solvent. Diethyl ether (Et_2O) was subsequently poured on the filtered CNTs, and vacuum was applied for 30 min after emptying the filtration flask. Finally, CNTs were scratched from the filter and dried under high vacuum. Dialysis of Ab-CNT samples was carried out with cellulose ester membranes with a 300 kDa MWCO (Spectrum Laboratories).

2.3.1. MWNT **3** and MWNT **4**

For the preparation of the carboxylated MWNTs, pristine MWNTs **1** and **2** (100 mg) were dispersed in 50 mL of an aqueous sulphuric acid/nitric acid mixture (3:1 v/v, 98% and 65%, respectively), and the dispersion was sonicated in a water bath for 24 h at a temperature below 50 °C. Deionized water was then carefully added to a final volume of 150 mL. The mixture was filtered over a PTFE membrane (0.1 μm), washed with H_2O until the filtrate reached a neutral pH, and then washed with MeOH and Et_2O. Finally, the CNTs were dried under high vacuum (weight yield: 84% and 70% for MWNT **3** and MWNT **4**, respectively).

2.3.2. MWNT **5**

MWNTs **3** (100 mg) were suspended in 100 mL of DMF and sonicated in water bath for 10 min. A solution of *N*-Boc-amino-diethoxy-ethylamino-acetic acid (100 mg) and paraformaldehyde (100 mg) in DMF was added. The suspension was sonicated for 10 min. The reaction mixture was heated at 125 °C for 24 h, while a solution of *N*-Boc-amino-diethoxy-ethylamino-acetic acid (100 mg) and paraformaldehyde (100 mg) in DMF were added after 2, 4, 6, and 8 h. After cooling to RT, the reaction mixture was filtered and then washed with DMF, MeOH and Et_2O and finally dried under high vacuum.

The *f*-MWNTs (50 mg) were suspended in dry DMF (5 mL). HOBt (67 mg, 496 μmol) and EDC (95 mg, 496 μmol) were added and the suspension was sonicated for 10 min. Pht-monoprotected triethylene glycol diamine derivative (200 mg, 510 μmol) and DIEA (170 μL) were dissolved in DMF (3 mL) and added to the reaction mixture. The reaction was stirred for 48 h at RT under argon. The reaction mixture was filtered and then washed with DMF, MeOH and Et_2O and finally dried under high vacuum.

2.3.3. MWNT **6**

MWNTs **4** (100 mg) were suspended in oxalyl chloride (20 mL), then DMF (0.4 mL) was added and the reaction was sonicated in a water bath for 30 min under Ar. Subsequently, the reaction was stirred at 60 °C under Ar for 24 h. After this period the solvent was dried under reduced pressure. The CNTs were suspended again in dry THF and Pht-monoprotected triethylene glycol diamine derivative (150 mg,

382 μmol) was added to the mixture, followed by sonication in a water bath for 30 min. Then the reaction mixture was heated at 70 °C under Ar for 48 h. After cooling to RT, the reaction mixture was filtered and then washed with DMF, MeOH and Et_2O and finally dried under high vacuum.

The *f*-MWNTs (100 mg) were then suspended in 100 mL of DMF and sonicated in a water bath for 20 min. The α-amino acid derivative (300 mg, 980 μmol) and paraformaldehyde (294 mg, 9.8 mmol) were added portion-wise over 2 days (1 addition per day) and the reaction mixture was heated at 120 °C for 2 days. After cooling to RT, the reaction mixture was filtered and then washed with DMF, MeOH and Et_2O and finally dried under high vacuum.

2.3.4. MWNT **7** and MWNT **8**

MWNTs **5** and **6** (40 mg), respectively, were dispersed in a solution of hydrazine hydrate (120 μL) in ethanol (20 mL) and sonicated in water bath for 20 min. The mixture was stirred overnight at RT and then it was filtered and washed with DMF, MeOH and Et_2O and dried under high vacuum. The compound was finally dialyzed against water (Regenerated cellulose membrane, MWCO = 12–14 kDa, Spectrum Laboratories) for 24–36 h and lyophilized. The degree of functionalization, determined by the Kaiser test, was 188 μmol/g and 115 μmol/g for MWNT **7** and MWNT **8**, respectively.

2.3.5. MWNT **9** and MWNT **10**

MWNTs **7** and **8** (50 mg), respectively, were dispersed in dry DMSO (5 mL) and neutralized with dry diisopropylethylamine (DIEA). A solution of DTPA dianhydride (91 mg, 255 μmol) in DMSO (5 mL) was added and the suspension was stirred for 48 h at 60 °C under Ar. The reaction mixture was filtered and then washed with DMSO, MeOH and Et_2O and finally dried under high vacuum. The degree of DTPA functionalization, determined by comparison of the Kaiser test value with the starting one, was 140 μmol/g (yield: 74%) and 48 μmol/g (yield: 42%) for MWNT **9** and MWNT **10**, respectively.

2.3.6. MWNT **11** and MWNT **12**

For deprotection of the Boc group, MWNTs **9** and **10** (40 mg) were dispersed in a 4 M HCl solution in dioxane (40 mL) sonicated for 30 min, and stirred at RT overnight. The CNTs were subsequently washed by filtration with DMF, MeOH and Et_2O and dried under high vacuum. The degree of functionalization determined by comparison of the Kaiser test value with the starting one was 140 μmol/g and 41 μmol/g for MWNT **11** and MWNT **12**, respectively.

2.3.7. MWNT **13** and MWNT **14**

MWNTs **11** and **12** (20 mg) were suspended in dry DMF and neutralized with dry DIEA (6 μL, 35 μmol). A solution of *N*-succinimidyl-3-maleimidopropionate (3.7 mg, 14 μmol) in DMF (2 mL) was added. The reaction was sonicated for 20 min and then stirred at RT under Ar for 48 h. The CNTs were washed by filtration with DMF, MeOH and Et_2O, and then dried under high vacuum. The degree of functionalization, determined by comparison of the Kaiser test value with the starting one, was 104 μmol/g (yield: 74%) and 13 μmol/g (yield: 32%) for MWNT **13** and MWNT **14**, respectively.

2.3.8. MWNTs **15** and **16**

The maleimido-derivatized MWNTs **13** and **14** (10 mg) were dispersed in 20 mL of IgG-SH solution (3 μM) in PBS (5 mM EDTA, pH 6.5) and the mixture was shaken for 24 h or 60 h, respectively, at RT. The CNTs were then centrifuged and washed thoroughly with PBS (pH 7.4) until there was no antibody detected in the supernatant by UV–vis spectroscopy. The resulting conjugates were dialyzed (MWCO 300,000 Da) against PBS (pH 7.4) for 24 h and then stored at 4 °C as dispersions of 0.5 mg/mL in PBS (pH 7.4). The degree of functionalization, determined by TGA, was 1.3 μmol of Ab per gram of CNTs and 0.6 μmol of Ab per gram of CNTs for MWNT **15** and MWNT **16**, respectively.

2.3.9. MWNTs **17** and **18**

The maleimido-derivatized MWNTs **13** and **14** (10 mg) were dispersed in 20 mL of Fab′-SH solution (8.4 μM) in PBS (5 mM EDTA, pH 6.5) and the mixture was shaken for 24 h or 37 h, respectively, at RT. The CNTs were then centrifuged and washed thoroughly with PBS (pH 7.4) until there was no Fab′ detected in the supernatant by UV–vis spectroscopy. The resulting Fab′–MWNT conjugates were dialyzed (MWCO 300,000 Da) against PBS (pH 7.4) for 24 h and then stored at 4 °C as dispersions of 0.5 mg/mL in PBS (pH 7.4). The degree of functionalization, determined by TGA, was 3 μmol of Fab′ per gram of CNTs and 1.4 μmol of Fab′ per gram of CNTs for MWNT **17** and MWNT **18**, respectively.

2.4. Characterization of antibodies and f-MWNTs

2.4.1. UV–vis–NIR microscopy

Spectra were recorded on a Cary 5000 spectrophotometer (Varian) using 1 cm path quartz cuvettes.

2.4.2. Ellman assay

The number of reactive sulfhydryl groups introduced onto the IgG was assessed by Ellman's assay [27]. A stock 0.01 M solution of 5,5′-dithio-*bis*-(2-nitrobenzoic acid) (DTNB) in PBS–EDTA–$NaHCO_3$ (pH 7.8) was prepared. 10 μL of DTNB stock solution were diluted with 500 μL of buffer and mixed with 50 μL of the IgG analyte solution. After incubation at RT for 15 min, the absorption spectrum of the solution was measured, using as a blank a solution obtained in the same way, adding 50 μL of buffer in place of the analyte solution. The maximum absorbance at 412 nm was measured to quantify the sulfhydryl groups in the analyte solution ($\varepsilon = 14{,}150\ M^{-1}\ cm^{-1}$), resulting in approximately 5 groups per IgG.

2.4.3. Kaiser test

Kaiser test (Kaiser test kit, Sigma–Aldrich) was performed to determine the degree of functionalization of the synthesized CNT constructs. In a typical test, 0.3–0.5 mg of CNTs were dispersed in a mixture of phenol (75 μL, 80% in ethanol) and KCN (100 μL in H_2O/pyridine) solution and sonicated for 2 min in an ultrasonic bath. Subsequently, 75 μL of ninhydrin solution (6% in ethanol) were added, and the mixture was heated at 120 °C for 10 min. It was then cooled and diluted with 60% ethanol in water to a final volume of 3 mL. After centrifugation (3000 rpm, 10 min), the absorption spectrum of the supernatant was measured, using as blank a solution obtained in the same way but without CNTs. The absorbance maximum at 570 nm was used to calculate the amine loading in the CNT samples ($\varepsilon = 15{,}000\ M^{-1}\ cm^{-1}$). Reported values are an average of at least two separate measurements.

2.4.4. Thermogravimetric analysis (TGA)

TGA was performed using a TGA Q500 (TA Instruments) with an isotherm run at 100 °C for 20 min (to remove residual solvent) and a ramp from 100 to 1000 °C at 10 °C/min, under N_2 with a flow rate of 60 mL/min. Reported graphs are an average of at least two separate measurements. The Ab- and Fab′-CNT samples (in PBS) were extensively washed with milliQ water by several cycles of centrifugation and removal of the supernatant, followed by a dialysis (12–14 kDa cut-off membrane), and subsequently lyophilized, prior to TGA analysis, in order to remove the salts present in the buffer.

2.4.5. Transmission electron microscopy (TEM)

The CNT samples were dispersed in water by sonication, and the dispersions were drop-casted onto carbon-coated copper grids (Formvar/Carbon 300 Mesh; Cu from Delta Microscopies) which were subsequently dried. The TEM analyses were performed using a Hitachi600 microscope with an accelerating voltage of 75 kV. Length and diameter measurements were performed using NIH ImageJ software.

2.4.6. Gel electrophoresis

Gel electrophoresis was performed using a Novex®8–16% Tris–Glycine gel (Life technologies) and run under either non-reducing or reducing conditions (by addition of 5% β-mercaptoethanol) using a mini-vertical electrophoresis system (XCell SureLock™, Life technologies). The gels were stained with Coomassie blue.

2.4.7. Surface plasmon resonance (SPR)

Surface plasmon resonance measurements were performed on a Biacore 3000 system (GE Healthcare). The sensor chip CM5, surfactant P20, amine coupling kit containing NHS and EDC•HCl were purchased from Biacore and streptavidin from Sigma–Aldrich. The antigen sequence ^{296}HGVTSAPDTRPAPGSTAPPA^{315}, which belongs to the antibody-recognized domain of polymorphic epithelial mucin (PEM), was synthesized, together with a control peptide (called "scrambled" antigen: APHADPSTPGAPSVTPRTAG) with the same number and type of amino acids, but placed at different positions in the sequence. HEPES-buffered saline (10 mM HEPES, 150 mM sodium acetate, 3 mM magnesium acetate, 0.005% surfactant P20, pH 7.4) was used as the running buffer. The sensor chip for the measurement was prepared as follows: the surface of a sensor CM5 chip was activated by EDC/NHS. Immobilization of streptavidin was performed by injection onto the activated surface with 35 μL of streptavidin (100 μg/mL in formate buffer, pH 4.3), which gave a signal of approximately 5000 RU, followed by 20 μL of ethanolamine hydrochloride (pH 8.5) to saturate the free activated sites of the matrix. Biotinylated antigen and scrambled antigen (1 μM in Hepes buffer) were allowed to interact with streptavidin until a response of 700 RU was obtained. The different analytes were dissolved/dispersed in the running buffer. Binding experiments were carried out at 25 °C at a constant flow rate of 20 μL/min. Different concentrations of Ab or Ab-CNTs were injected for 3 min, followed by a dissociation phase of 3 min. The sensor chip surface was regenerated after each experiment by injection of 10 μL of 10 mM HCl.

2.5. Radio-labelling of DTPA–MWNT conjugates

For the biodistribution studies, the DTPA–MWNT conjugates were radiolabelled with ^{111}In using a standard procedure optimized by our laboratories previously [28]. The radioactive tracer [^{111}In]Cl_3 was obtained from Amersham Pharmacia Biosciences as an aqueous solution and used without further purification. In brief, well-dispersed DTPA–MWNTs (500 μg/mL) were diluted with an equal volume of 0.2 M ammonium acetate buffer (pH 5.5), to which $^{111}InCl_3$ was added. DTPA–MWNT–^{111}In mixture solutions were mixed by vortexing every 5 min for

30 min at room temperature. The reaction was quenched by the addition of 0.1 M EDTA chelating solution. $^{111}InCl_3$ alone was also subjected to the same conditions of the labelling reaction as a control. Excess unreacted ^{111}In was removed by centrifugation of the [^{111}In]DTPA–MWNTs and the pellets were recovered which contained the [^{111}In]DTPA–MWNT fraction only. Further centrifugation was carried out prior to injection in order to ensure the absence of free ^{111}In or [^{111}In]DTPA. The labelling efficiency was analyzed by spotting the [^{111}In]DTPA–MWNTs on thin layer chromatography (TLC) strips (Agilent Technologies UK Ltd., Stockport). TLC strips were developed with a mobile phase of 50 mM EDTA in 0.1 M ammonium acetate and allowed to dry before analysis. The auto-radioactivity of each strip was developed and counted quantitatively using a Cyclone phosphor detector (Packard Biosciences).

2.6. Pharmacokinetics and tissue biodistribution of [^{111}In]DTPA–MWNT conjugates in mice by gamma scintigraphy

All *in vivo* experiments were conducted under the authority of project and personal licences granted by the UK Home Office and the UKCCCR Guidelines (1998). The pharmacokinetic studies including the blood circulation and the excretion profiles of different radio-labelled *f*-MWNTs, as well as the biodistribution in major organs were carried out using normal C57/Bl6 mice. The two types of *f*-MWNTs and their IgG and Fab′ conjugates (6 conjugates in total) were examined. The [^{111}In]DTPA–MWNTs were centrifuged and re-suspended in 5% dextrose solution (isotonic) for injection to mice.

Mice were given 50 μg [^{111}In]DTPA–MWNTs intravenously *via* the tail vein. The blood clearance profiles were established by collecting blood samples in heparinised capillaries from 2 min up to 24 h after injection and counted by γ-scintigraphy (LKB Wallac 1282 Compugamma, PerkinElmer).

To obtain the excretion profile, mice were housed singly in metabolic cages in which animals had free access to water but not food. After 24 h, urine and faeces were collected from individual cages and counted by γ-scintigraphy.

For tissue biodistribution study, major organs including skin, liver, spleen, heart, lung, muscle, bone, brain, stomach and intestine were obtained post mortem at 1, 4 and 24 h after injection of [^{111}In]DTPA–MWNTs. Tissues were weighed and the radioactivity was measured by γ-scintigraphy. The percentage injected dose per gram tissue was calculated for each organ. Four animals were used for each time point for every material.

2.7. Whole body 3D SPECT/CT imaging of mice injected with [^{111}In]DTPA–MWNT conjugates

Whole body imaging of [^{111}In]DTPA–MWNTs was carried out using SPECT/CT imaging technique. Mice were anaesthetized by isoflurane inhalation. Each animal was injected intravenously with 50 μg of [^{111}In]DTPA–MWNTs containing approximately 5–6 MBq. Immediately after injection (up to 0.5 h) and at 4 h and 24 h, mice were imaged using the Nano-SPECT/CT scanner (Bioscan). SPECT images of each mouse were taken in 24 projections over 30–40 min using a four-head scanner with 1.4 mM pinhole collimators. CT scans were performed at the end of each SPECT acquisition. After the reconstruction of all images with MEDISO software (Medical Imaging Systems), SPECT and CT images was merged using the InVivoScope™ software (Bioscan).

3. Results

3.1. Double chemical functionalization of multi-walled carbon nanotubes

Double functionalized conjugates were prepared using two different strategies (Scheme 1) in order to functionalize the MWNTs with the IgG or its fragment Fab′ and with the chelating agent required to trap the radionuclide for *in vivo* localization of the hybrids. Covalent conjugation of IgG or Fab′ was employed to guarantee final constructs with good stability, minimizing

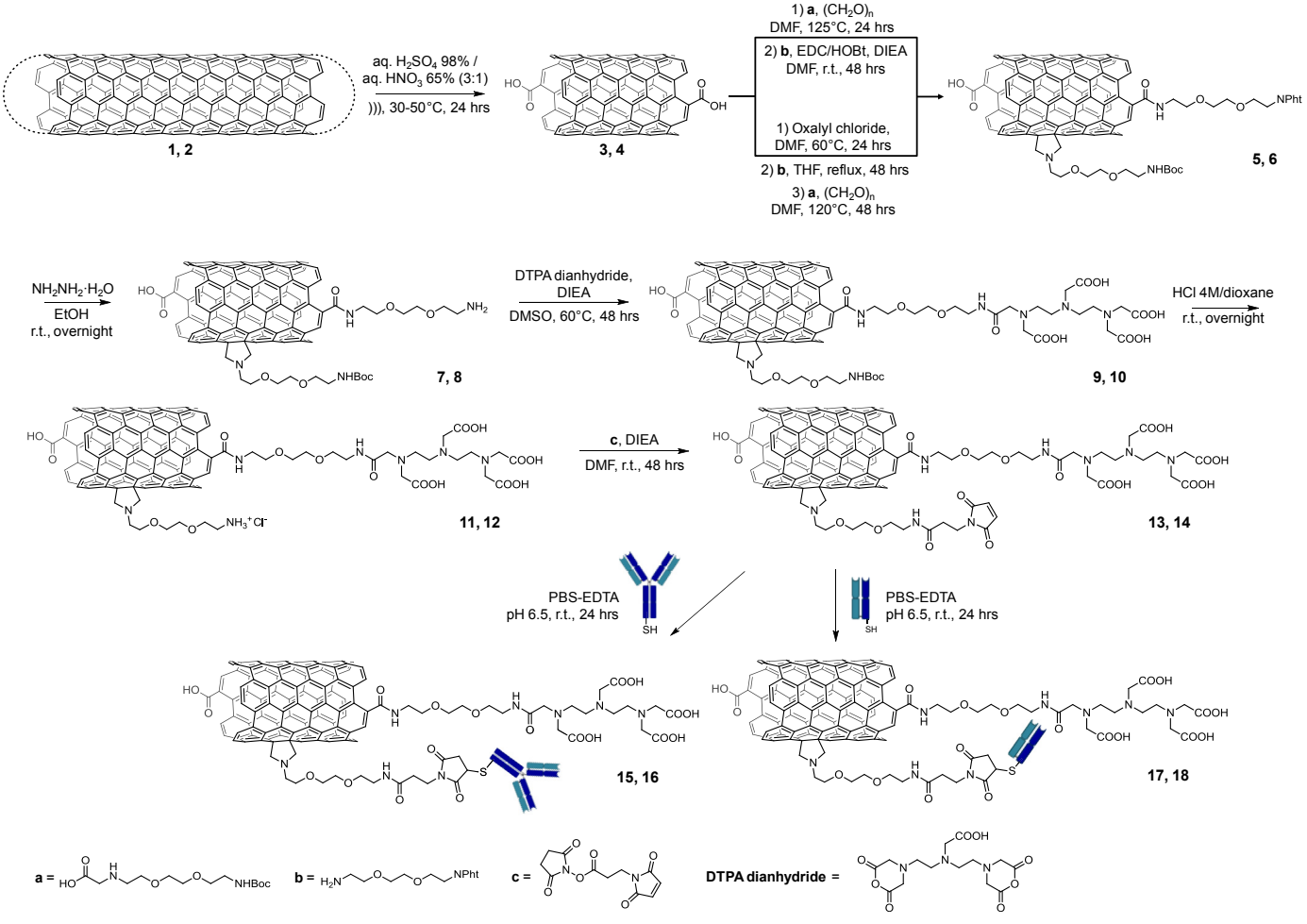

Scheme 1. Synthesis of *f*-MWNTs.

Table 1
MWNT characteristics.

f-MWNTs	Mean diameter[a] (nm) ± S.D.	Mean length[a] (nm) ± S.D.	Total functionalization degree (amidation + cycloaddition)[b] (μmol/g of CNTs)	DTPA loading[b] (μmol/g of CNTs)	Antibody loading[c] (μmol/g of CNTs)
N-MWNT **11**	9.2 ± 2.7	396 ± 290	328 (188 + 140)	140	–
N-MWNT **15**	9.2 ± 2.7	396 ± 290	328 (188 + 140)	140	13
N-MWNT **17**	9.2 ± 2.7	396 ± 290	328 (188 + 140)	140	3
W-MWNT **12**	39.5 ± 8.5	268 ± 174	156 (115 + 41)	48	–
W-MWNT **16**	39.5 ± 8.5	268 ± 174	156 (115 + 41)	48	0.6
W-MWNT **18**	39.5 ± 8.5	268 ± 174	156 (115 + 41)	48	1.4

[a] Analyzed by TEM measurements of MWNTs **3** and **4** ($n = 100 - 160$).
[b] Assessed by Kaiser test.
[c] Assessed by TGA.

dissociation or possible displacement by other biomolecules *in vivo*.

First of all, both types of pristine MWNTs (*N*-MWNT **1** and *W*-MWNT **2**) underwent an oxidative cutting step using a mixture of aqueous sulphuric and nitric acid under sonication for 24 h. This treatment shortens the nanotubes, improves their dispersibility in water, and introduces carboxylic groups on their surface that can be derivatized by amidation. The oxidized MWNTs were then

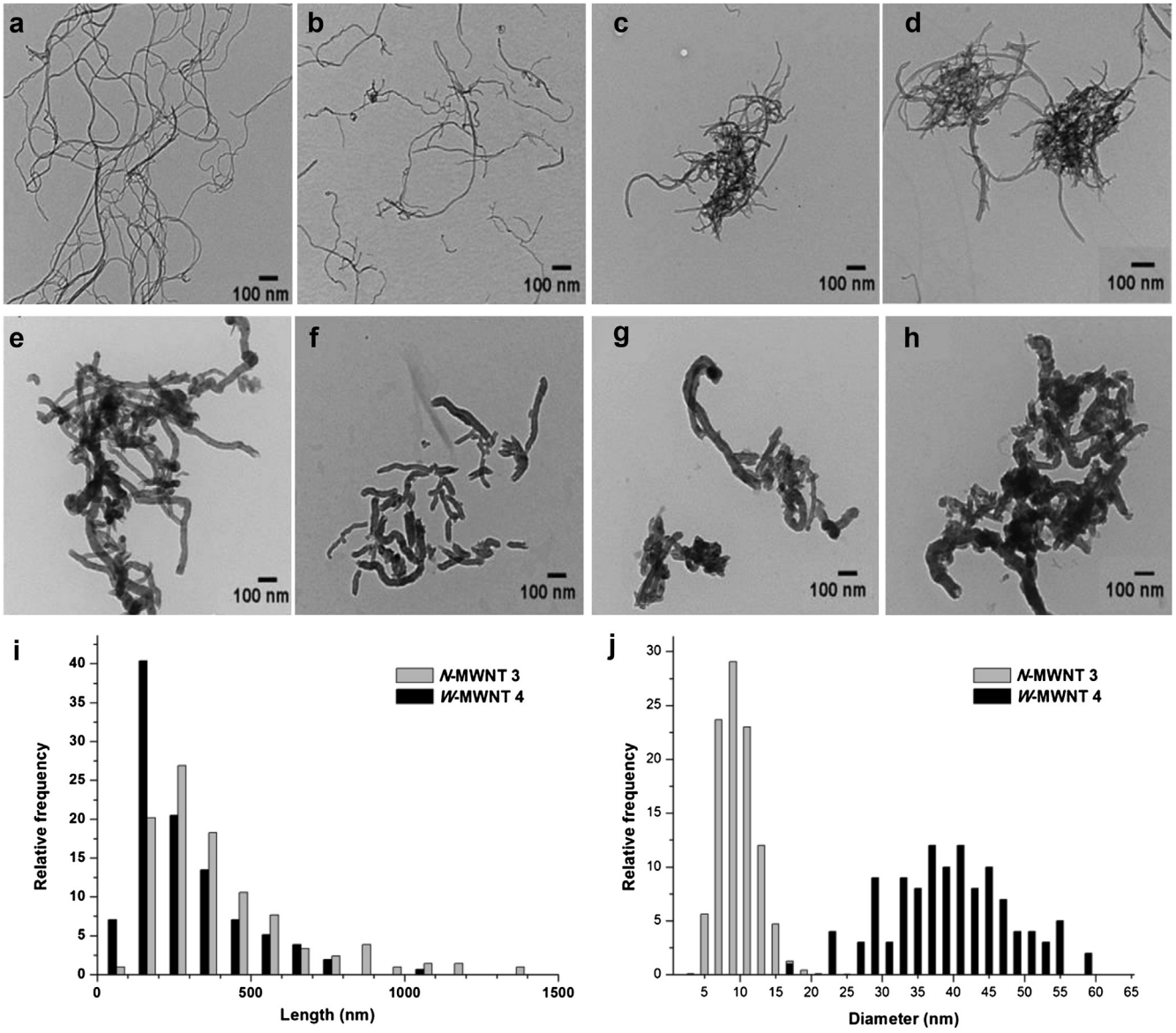

Fig. 1. Morphological characterization of pristine and *f*-MWNTs. (a–d) TEM images of *N*-MWNT **1**, **3**, **15** and **17**. (e–h) TEM images of *W*-MWNT **2**, **4**, **16** and **18**. (i–j) Histograms of the length and diameter distribution of *N*-MWNT **3** and *W*-MWNT **4**. Measurements were taken from at least 100–200 nanotubes.

functionalized in two consecutive steps *via* amidation and 1,3-dipolar cycloaddition of azomethine ylide to introduce two orthogonally protected amine-terminated linkers (Scheme 1). The phthalimide-protected amine was selectively deprotected with hydrazine and reacted subsequently with DTPA dianhydride. Afterwards, the second amine was deprotected by cleavage of the Boc group in acidic conditions. Both *N*-MWNTs and *W*-MWNTs were modified upon reaction with *N*-hydroxysuccinimide-activated propionic acid bearing a maleimide group. The obtained maleimide-functionalized *N*-MWNT **13** and *W*-MWNT **14** were conjugated to the IgG and Fab′ (containing free thiols generated as described below) *via* the formation of stable thiol-ether bonds. The IgG was treated with 2-iminothiolane (Traut's reagent [29]) to introduce sulfhydryl groups, as previously described [30]. The Fab′ molecule was engineered to contain a single unpaired cysteine residue at the C terminus of the heavy chain that was available for conjugation. During the preparation of the Fab′ there was some spontaneous dimerization of the molecule *via* the formation of a disulphide bond between these unpaired cysteine residues. Before coupling to functionalized nanotubes a mild reduction was performed (using 2 mercaptoethylamine) to reverse the dimerization. The formation of monomers was monitored by gel electrophoresis. The coupling reaction between maleimide-functionalized MWNTs and the thiolated IgG and Fab′ was performed by mixing the two components in PBS–EDTA at pH 6.6, and gently shaking the mixture at room temperature (Scheme 1). To follow the coupling reaction, a small aliquot of the reaction mixture at different time points was centrifuged to precipitate the CNTs. The concentration of IgG or Fab′ in the supernatant, corresponding to the unreacted antibody fragments, was determined by measuring the absorbance at 280 nm. When the coupling was complete, the reaction was stopped and the mixture was thoroughly washed with fresh PBS at pH 7.4, by several cycles of centrifugation and removal of the supernatant. Dialysis was performed against PBS at pH 7.4 using a membrane with a cut-off of 300 kDa, to ensure the complete removal of unbound proteins from *W*-MWNT **16**/**18** and *N*-MWNT **15**/**17**. The Kaiser test was used to assess the degree of functionalization after each step (Table 1). A lower functionalization degree was observed for *W*-MWNTs with respect to *N*-MWNTs, but the values correlate well considering the differences in the surface area for the two types of CNTs (specific surface areas given by the suppliers are: 110–130 m^2/g for *W*-MWNTs, 250–300 m^2/g for *N*-MWNTs). The amounts of IgG or Fab′ in the conjugates were determined by TGA. The results are summarized in Table 1. Considering the antibody loading for IgG bearing MWNTs (**15** and **16**) and for Fab′ bearing ones (**17** and **18**), it should be underlined that each IgG bears two Fab′ units, and thus the degree of functionalization expressed as μmol of antibody per gram of MWNT should be normalized per Fab′ units, in order to make the comparison meaningful. As a consequence, i.e. doubling the values obtained for the IgG MWNT, the degree of functionalization of IgG and Fab′ MWNT conjugates appeared to be almost the same.

3.2. Characterization of doubly functionalized multi-walled carbon nanotubes

3.2.1. Transmission electron microscopy (TEM)

The *f*-MWNTs were characterized by transmission electron microscopy (TEM). Both types of *f*-MWNTs were well-dispersed and the TEM images clearly showed that the CNT structure was preserved throughout the whole synthetic procedures (Fig. 1). TEM micrographs of pristine *N*-MWNT and *W*-MWNT, the oxidized precursors (*N*-MWNT **3** and *W*-MWNT **4**), IgG conjugates (*N*-MWNT **15** and *W*-MWNT **16**) and Fab′ conjugates (*N*-MWNT **17** and *W*-MWNT **18**) are displayed in pairs in Fig. 1a & e, 1b & f, 1c & g, and 1d & h, respectively. All appeared as tangled tubes with obvious differences in their diameter. Fig. 1i and j presents the length and diameter distribution histograms with measurements based on ImageJ analysis of the TEM images. Both types of *f*-MWNTs showed similarity in length (Fig. 1i) in contrast to the significant difference in the diameter (Fig. 1j). 1,3-Dipolar cycloaddition and amidation reactions are not expected to affect the length and diameter of the nanotubes as the length is controlled by the acid treatment. A summary of mean values for *N*-MWNT and *W*-MWNT length and diameter is reported in Table 1. As a result, *N*-MWNT exhibited a much higher aspect ratio (43.0) compared to *W*-MWNT (6.8) as calculated from the mean values.

3.2.2. Gel electrophoresis

Gel electrophoresis was performed in both reducing and non-reducing conditions to examine the covalent bonding between the antibody fragments and the CNTs, and to confirm the complete removal of any adsorbed proteins after the washing treatments. *f*-MWNTs stayed in the loading well and only the unbound material could move. When the gel was run in non-reducing conditions, no IgG or Fab′ was detected (Fig. S1). On the other hand, when the gel was run after incubation with 2-mercaptoethylamine, inducing the reduction of the disulfide bond between the heavy and light chains, protein fragments were observed. It should be noted that a much higher concentration of reductant was used to provide such reducing condition while the preparation of the thiolated IgG and Fab′ derivatives for MWNT conjugation was performed using a low concentration of 2-mercaptoethylamine so that the interchain disulphide bonds were not broken. A negative control was also included in which MWNT **8** (not presenting the maleimide functionality) was treated with Fab′ and then washed following the same protocol used for the covalent reaction. No protein material was detected in the gel under both non-reducing and reducing conditions, confirming the efficacy of the washing treatments to remove any adsorbed proteins, and thus the covalent nature of the bond between the antibody fragments and the CNTs (data not shown).

3.2.3. Thermogravimetric analysis (TGA)

The degree of functionalization was evaluated using TGA performed under inert atmosphere (Fig. 2 and Fig. S2). The increase in

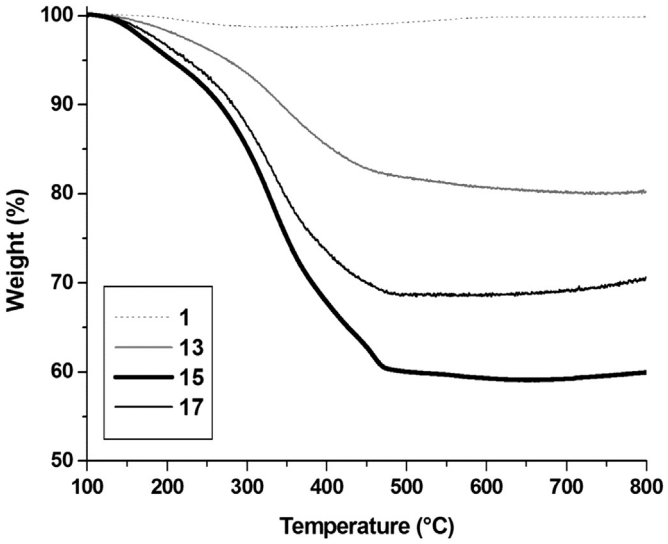

Fig. 2. Thermogravimetric analysis of *N*-MWNT **1** (dotted line), **13** (grey), **15** (black thin line) and **17** (black thick line) under N_2. The weight loss was calculated at 600 °C.

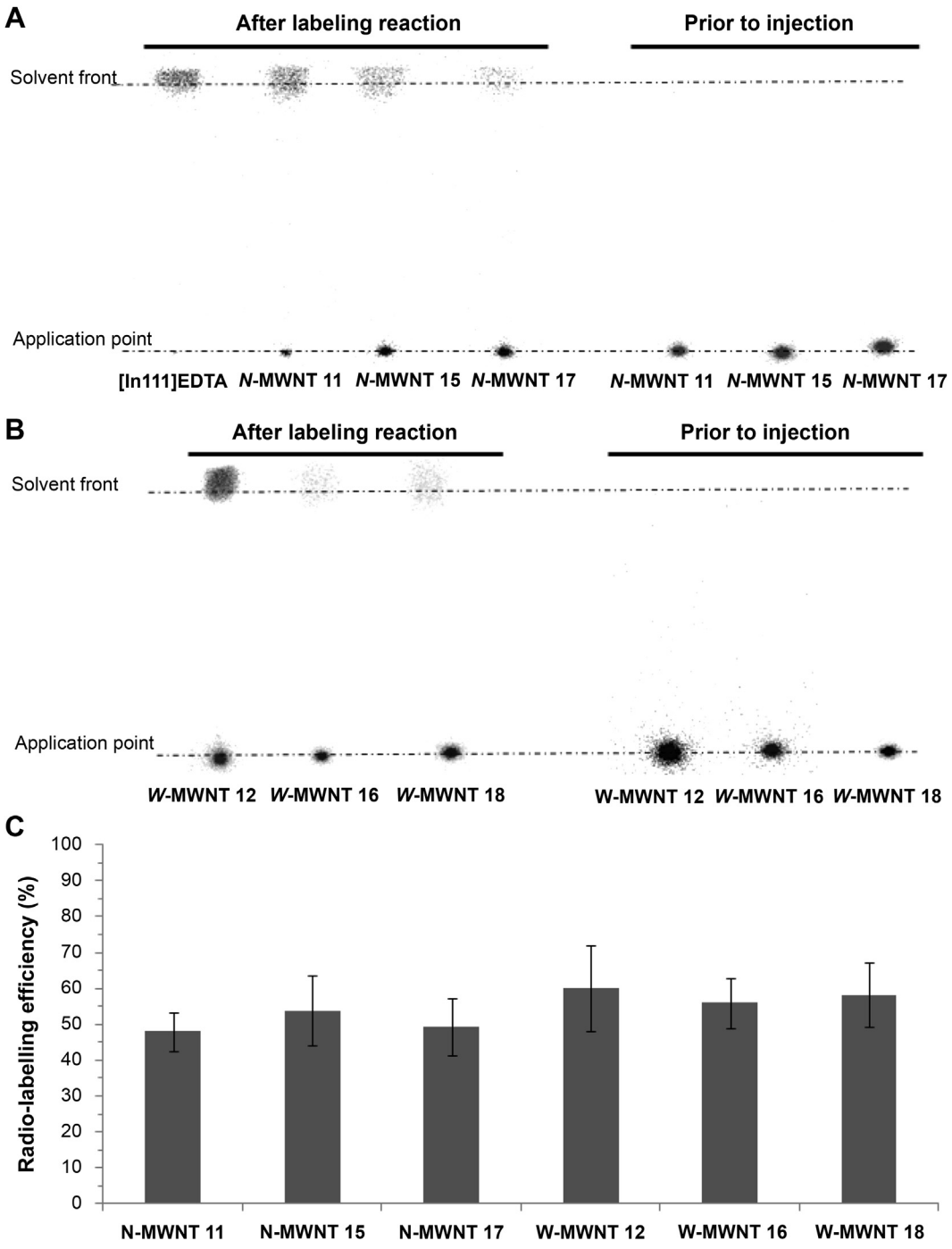

Fig. 3. Radio-labelling efficiency of DTPA–MWNT conjugates. TLC strips of (A) Narrow and (B) Wide [^{111}In]DTPA–MWNT, IgG and Fab′ conjugates immediately after radio-labelling reaction and quenching by EDTA (left) and prior to injection (right). (C) A summary of the radio-labelling efficiency obtained from 3 different reactions. The values are presented as mean ± S.D.

the weight loss for the final conjugates in reference to their precursors corresponded to the amount of IgG or Fab′ bound to the MWNTs (Table 1). The results correlate well with gel electrophoresis where the relative intensity of the bands gave an indication about the quantity of loaded IgG and Fab′.

3.2.4. Surface plasmon resonance (SPR)

The functional activity of the IgG and its fragment coupled to carbon nanotubes was also assessed. It is of paramount importance to make sure that these biomolecules are still biologically active. In this context, the antigen-recognition capability of the CNT-coupled antibody was verified by surface plasmon resonance (SPR). This technique allows real-time measurements of the specific interactions between the antibody and its antigen [31,32]. The sensorgrams showed that all conjugates were able to recognize the specific antigen immobilized on the sensor chip in a dose-dependent manner (Fig. S3) [28]. However, it is worth pointing out that it is not possible to make quantitative analysis of the binding interaction for antibody-CNT constructs using SPR. The two main reasons are: 1) the precise molecular weight for CNTs, being

heterogeneous materials, cannot be determined and hence the association and dissociation rate constants could not be obtained from the sensorgrams; 2) the antibodies are likely to be randomly distributed in the conjugates, and this may affect their overall binding capability. Nevertheless, the results highlight that the antigen-recognition capability of the antibodies were preserved after the covalent attachment onto CNTs.

3.3. Radio-labelling efficiency of the f-MWNT conjugates

The DTPA–MWNT conjugates were radio-labelled with γ-emitter ^{111}In in order to track their organ biodistribution *in vivo*. The labelling efficiency was examined by thin layer chromatography (TLC). Fig. 3 shows images of the TLC strips of different *N*-MWNTs (**11**, **15**, **17**) and *W*-MWNTs (**12**, **16**, **18**) conjugates immediately after labelling and prior to injection (within 24 h after labelling). The spots at the application point correspond to the *f*-MWNTs radio-labelled with ^{111}In, while free ^{111}In can be found at the solvent front. Unbound ^{111}In was removed by centrifugation and a subsequent washing step. Prior to injection, all conjugates were captured at the application point indicating the absence of free ^{111}In in the injected [^{111}In]DTPA–MWNTs.

The radio-labelling efficiency was expressed as % of [^{111}In] bound to the MWNTs in relation to total [^{111}In] (bound plus free [^{111}In]) in the sample. Fig. 3C shows that approx. 50% labelling efficiency was achieved for all *f*-MWNT conjugates. The stability of the radio-labelling was examined at 24 h post-incubation (after removal of unbound ^{111}In) in PBS or 50% serum. Results have shown that the [^{111}In]DTPA–MWNT conjugates remained stable for at least 24 h as only a negligible amount or no free ^{111}In was detected (Fig. S4).

3.4. Blood clearance and excretion profiles of the f-MWNT conjugates in mice

The blood clearance profiles of the *N*-MWNTs **11**, **15**, and **17** and *W*-MWNTs **12**, **16**, and **18** after intravenous (i.v.) injection are presented in Fig. 4A and B, respectively. Overall, all *f*-MWNTs displayed fast clearance from the circulation within the first 1 h. In the case of narrow nanotubes, *N*-MWNT **17** (Fab′-conjugated) showed significantly ($p < 0.03$) lower blood concentration at 2 min than the other *N*-MWNT derivatives (Fig. 4A, dark grey line). For the wide MWNT conjugates, *W*-MWNT **16** exhibited a significant rapid blood clearance within 5 min post-injection (Fig. 4B, light grey line) ($p < 0.005$).

To study the excretion profile of the *f*-MWNT conjugates, animals were housed in metabolic cages (one mouse per cage) and the urine and faeces were collected at 24 h post-administration followed by γ-scintigraphy (Fig. S5). It was found that negligible amounts (<1% of total injected dose) were eliminated into faeces in all cases. In general, a higher amount of the *W*-MWNT derivatives was detected in the urine compared to the *N*-MWNT derivatives. For example, around 5.2% of the injected dose of *W*-MWNT **12** was obtained in the urine, whereas only 1.3% of *N*-MWNT **11** (the thin counterpart) followed renal elimination.

3.5. Organ biodistribution of the f-MWNT conjugates in mice

The biodistribution of *N*-MWNT (**11**, **15**, **17**) and *W*-MWNT (**12**, **16**, **18**) conjugates in major organs in mice was assessed at 1 h, 4 h and 24 h after i.v. injection (Fig. 5 and Fig. S5). As shown in Fig. 5, the two series of *f*-MWNTs exhibited marked differences in the organ biodistribution. In the animals treated with *N*-MWNTs (**11**, **15**, **17**), the lung uptake, expressed as percentage of injected dose per gram of tissue, was significantly higher than the ones that

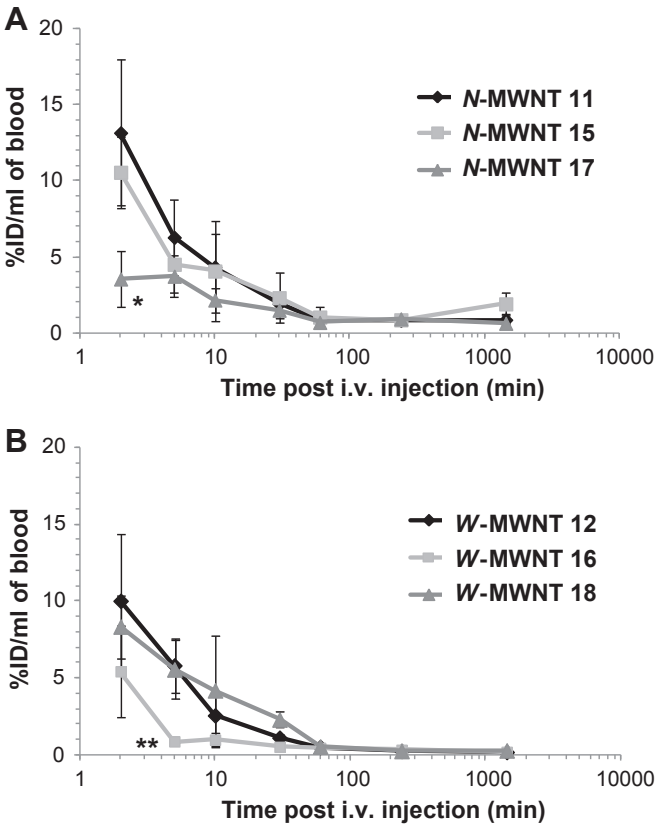

Fig. 4. Blood clearance profile of [^{111}In]DTPA–MWNT conjugates. (A) Narrow and (B) Wide *f*-MWNT conjugates in the blood of C57/Bl6 mice. Animals were injected with 50 μg of *f*-MWNT conjugates *via* a tail vein. The values are presented as mean ± S.D. ($n = 3$–4). $^{*}p < 0.03$; $^{**}p < 0.005$ (Student's *t*-test).

received *W*-MWNTs (**12**, **16**, **18**) by several orders of magnitude. Nevertheless, the accumulation in liver and spleen was relatively similar between the two classes of MWNTs. A gradual reduction in lung accumulation occurred for all the conjugates, while less significant changes were observed in the cases of liver and spleen. In contrast to *W*-MWNTs, *N*-MWNTs also exhibited some uptake in other tissues, despite two types of *f*-MWNTs were mostly found to accumulate in liver, spleen and lung (Fig. 5 and Fig. S6). Consistent results were obtained by SPECT/CT imaging.

3.6. Whole body 3D SPECT/CT imaging of mice injected with the f-MWNT conjugates

Whole body SPECT/CT imaging was carried out within 30 min, at 4 h and 24 h after i.v. injection of the six *f*-MWNT derivatives. As shown in Fig. 6, the results correlate well with the biodistribution profile assessed by γ-scintigraphy. The *N*-MWNTs (**11**, **15**, **17**) predominantly accumulated in liver, lung and spleen (Fig. 6A) while the *W*-MWNTs (**12**, **16**, **18**) were mainly detected in liver and spleen (Fig. 6B). Spleen exhibited brighter signals than the liver particularly for the *W*-MWNTs (**12**, **16**, **18**), which agrees with the higher %ID per gram of spleen compared to the liver obtained by γ-scintigraphy. SPECT signals were also detected in the bladder at early time point (less than 30 min) for all the conjugates suggesting a rapid clearance of a fraction of the injected conjugates through the urine.

4. Discussion

f-CNTs have been proposed as one of the most promising drug delivery nanomaterials in biomedicine. The rationale for this stands

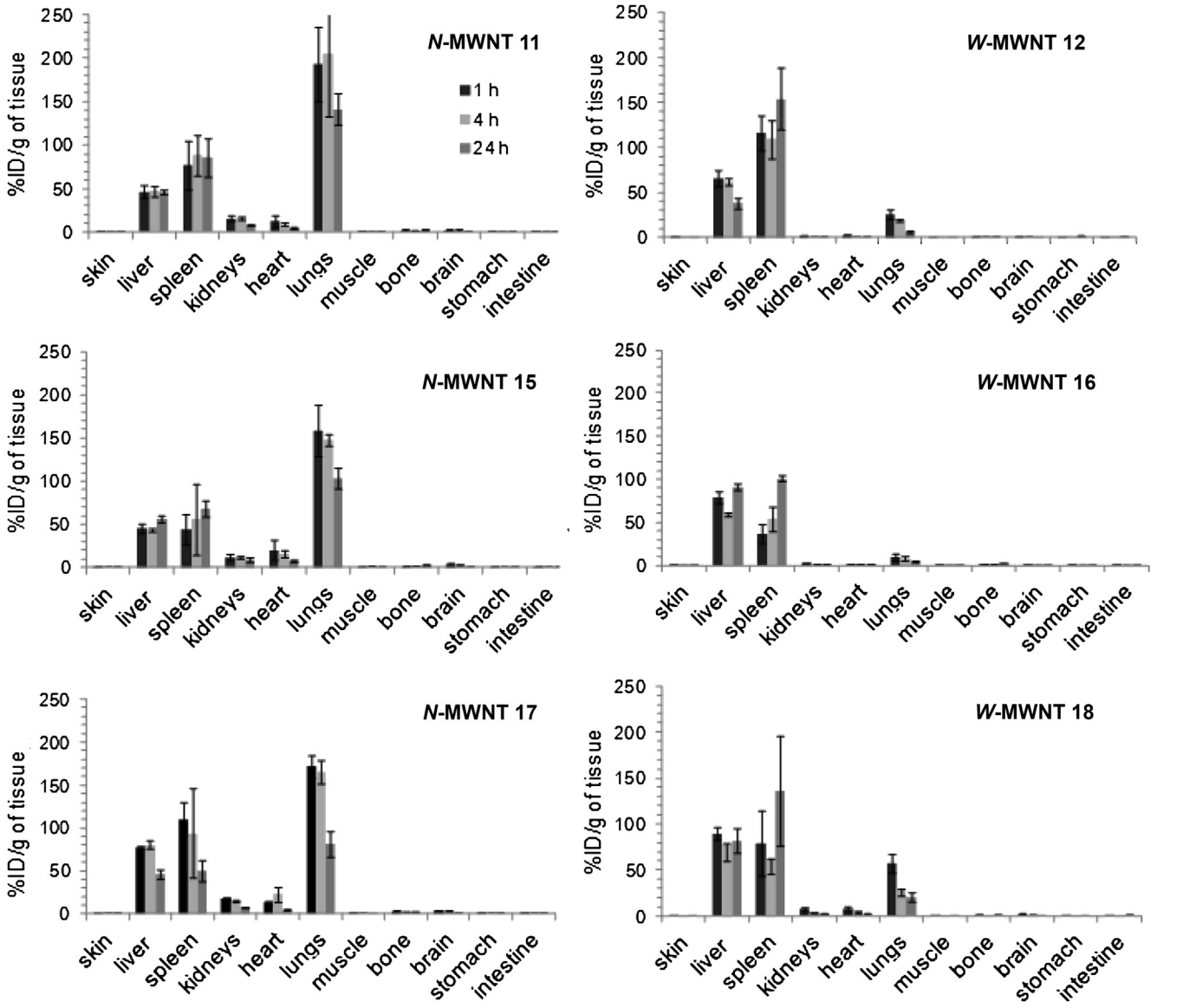

Fig. 5. Organ biodistribution of *f*-MWNT conjugates in C57/Bl6 mice. Animals were injected with 50 μg (250 μL) of *f*-MWNT conjugates intravenously *via* a tail vein. Radioactivity was measured in selected major organs by γ-scintigraphy at each time point. Data are presented as mean ± S.D. ($n = 3–4$).

on their high aspect ratio characteristics. Since CNTs possess large surface area including the inner core and outer tube surface, they can be functionalized with a wide variety of therapeutic or imaging agents [6]. Moreover, it has been found that the needle-like structure enables *f*-CNTs to enter cells *via* an energy-independent mechanism [33].

Recently, we investigated the influence of the degree of chemical functionalization of *f*-MWNTs on their tissue biodistribution [34]. In this previous study, three *f*-MWNT derivatives with increased number of surface functional groups were compared with regard of their pharmacokinetic profiles after i.v. administration in mice. The study concluded that the degree of chemical functionalization, which affects the individualization of CNTs, played a major role in determining the fate and organ biodistribution profile of *f*-MWNTs. The present study expanded the previous structure-function investigations further by exploring how the *f*-MWNT diameter can alter their organ biodistribution profile *in vivo*. Complete characterization, radio-labelling, and pharmacokinetic profiling of six double functionalized MWNTs possessing two remarkably different diameters (39.5 nm *vs* 9.2 nm) and three types of surface substitution (i.e. amino-functionalized, IgG- and Fab′-conjugated) were carried out and compared. All conjugates achieved comparable degree of chemical functionalization. The conjugates were administered *via* the i.v. route, enabling a direct comparison with the results from our previous studies [32].

As clearly shown in Fig. 5 and Fig. S6, all the *N*-MWNTs showed higher affinity to lung, bone and organs such as brain, kidney and heart compared to the *W*-MWNTs. Despite such significant difference may appear to be low, brain uptake values recorded for *N*-MWNT 17 and *W*-MWNT 18 at 1 h post-injection were 1.4 ± 0.5 and 0.8 ± 0.2 %ID/organ respectively, which are comparable or higher than the values reported in other studies that used nanoparticles to target brain *in vivo* [35]. Since the two types of MWNTs possess similar degree of functionalization and dispersibility, the distinct difference in the diameter of the tubes (i.e. exhibited the 4 times larger average diameter for the *W*-MWNTs compared to the *N*-MWNTs) seemed to be the key parameter leading to the marked

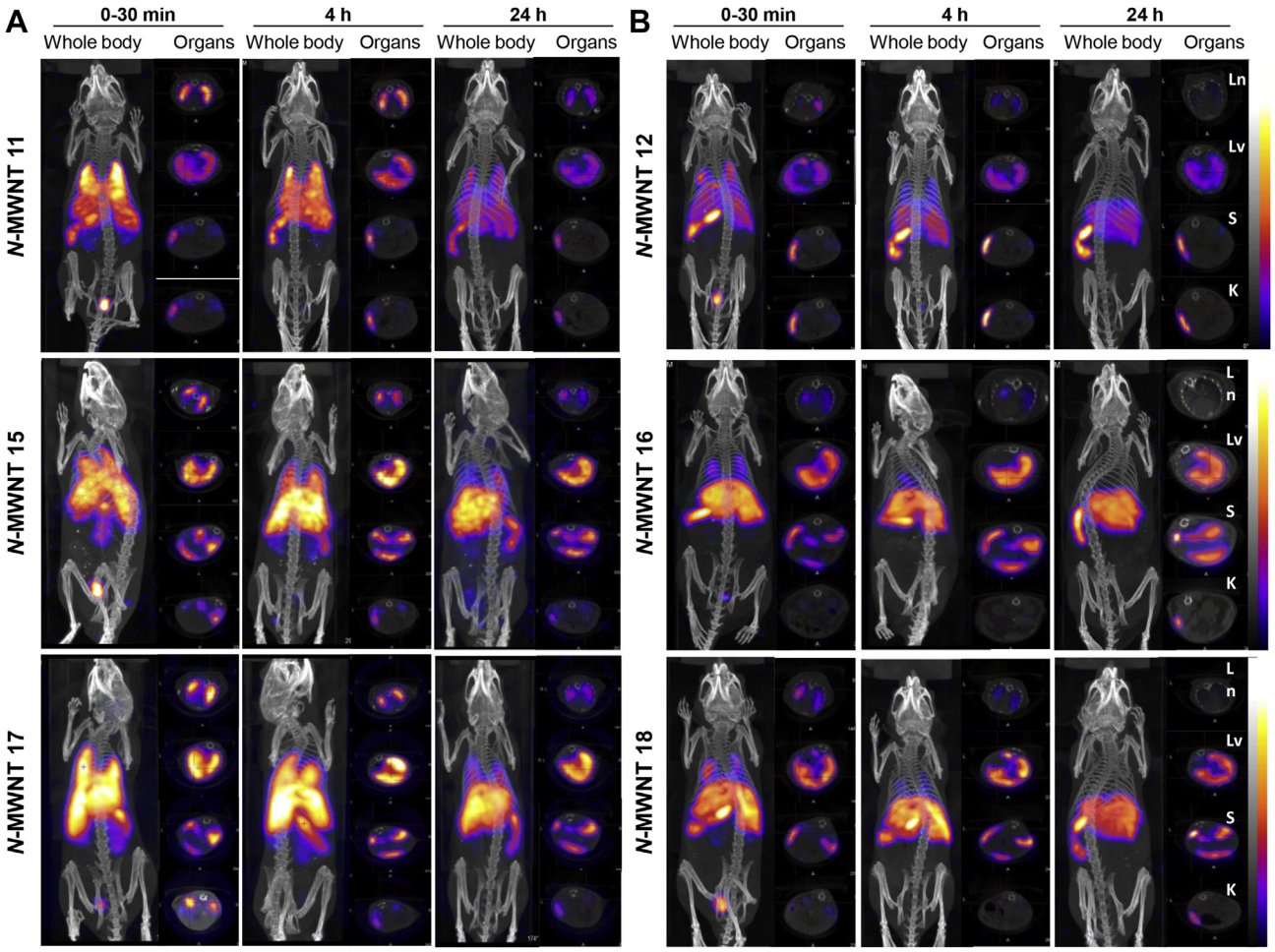

Fig. 6. Whole body 3D SPECT/CT imaging of mice at various time points following i.v. injection of (A) *N*-MWNT (**11**, **15**, **17**) and (B) *W*-MWNT (**12**, **16**, **18**) in C57/Bl6 mice. The whole body SPECT/CT image is presented in the left panel and the transverse images of selected organs are presented in the right panel in the order of lung (Ln), liver (Lv), spleen (S) and kidney (K).

differences in their organ biodistribution. Some studies have investigated the diameter of CNTs as a determining factor in inducing lung toxicity [24,25]. However contradictory conclusions were reported. This was mainly due to variations in the types of MWNTs used (e.g. suppliers and purification methods), the route of administration and the toxicity assay. Moreover, none of the CNTs used in those studies was chemically functionalized. To our knowledge, no previous studies have been conducted to directly compare the organ biodistribution profile of *f*-MWNTs as a function of their diameter and surface derivatization.

All the *f*-MWNTs studied here were removed from the blood circulation within the first hour post-injection. Thus, the enhanced tissue affinity of the *N*-MWNTs compared to the *W*-MWNTs for the non-reticular organs could not be attributed to higher concentrations in the blood. But, it could be related to the structure of the *N*-MWNTs which could favour interactions with biological compartments.

The exact reasons behind the advanced affinity of the *N*-MWNT series over the *W*-MWNT series to non-mononuclear phagocyte system (MPS) tissues are not yet known. It is possible that the alveolar macrophages might play a role in high lung uptake. Nevertheless, lung accumulation has been demonstrated in our previous study [23]. The fact that *N*-MWNT had higher affinity to lung is reminiscent of the data obtained with *f*-SWNT in our previous study [23]. Future work is needed to understand if lung uptake of *f*-MWNT is dependent on their diameter. However, it can be hypothesized that due to their narrow diameter and high aspect ratio, *N*-MWNTs could exhibit efficient interactions with biological membranes of non-reticular tissues in addition to passive accumulation in MPS organs (i.e. liver and spleen). The effect of diameter was studied and compared between the two series of conjugates where other parameters such as the length, degree of functionalization and the type of surface derivatization were similar.

It was not surprising that the *f*-MWNTs used in this study can pass through the glomerular filter since the glomerular filtration cut-off size is 30–40 nm (minimum diameter of fenestra is 30 nm; the width of epithelial podocyte filtration slits is 40 nm) [36]. Rapid renal clearance has been described in the case of *f*-SWNTs [37,38]. We have also previously reported renal excretion of *f*-MWNTs and *f*-SWNTs [17,28,34,39]. The presence of *f*-MWNTs was also confirmed by TEM examination of urine samples [28]. In this study, both *N*-MWNTs and *W*-MWNTs were excreted into urine without significant differences in terms of the amount excreted.

It was previously reported that antibody-conjugated CNTs showed high liver accumulation [22]. In this study, we report comparable levels of liver and spleen accumulation for all the conjugates without obvious hepatic clearance within the first 24 h post-administration. Transient reduction in lung uptake was observed for all of the *f*-MWNTs studied and some of them

exhibited a gradual increase in spleen uptake (Fig. 5). Many studies by us and others have reported lung to spleen translocation and hypothesized an association with lymphatic drainage [34,40,41].

The results also showed that the surface substitution with IgG or Fab′ biomolecules had minimal effects on the organ biodistribution of CNTs. It is possible that the loading of these biological ligands was not high enough to alter the biodistribution pattern. In other words, the dimensions of the carbon backbone as well as the degree of functionalization remained the main driving forces that influenced their biological behaviour. A few studies coupling antibodies to CNTs have demonstrated tumour targeting *in vivo* [22,42]. The antigen specificity of the studied antibody-conjugated MWNTs may become profound when using tumour-bearing models where MWNT conjugates can potentially target tumours that often overexpress MUC1. Nevertheless, tumour targeting is not the focus of the current study and future work will be conducted using MUC-1 tumour-bearing mice.

In conclusion, the present study compared the pharmacokinetic profiles of different *f*-MWNT derivatives with major differences in their diameters and surface derivatization. The results clearly demonstrated that the MWNT diameter is a critical factor that impacts organ biodistribution *in vivo,* in addition to the degree of chemical functionalization we previously reported. *f*-MWNTs of narrow diameters exhibited enhanced tissue affinity compared to the wider nanotubes. Further studies at the ultra-structural levels (e.g. TEM examination) of the *ex vivo* tissues would be key experiments to perform in the future to establish the nature of interactions between these two different types of *f*-MWNTs and biological membranes. Altogether, the present study gives a new insight into the design of *f*-MWNTs as carriers for diagnosis and therapy.

5. Conclusions

The *in vivo* biodistribution profiles of two types of MWNTs with distinct differences in diameters were investigated in this study. Both MWNTs were doubly functionalized *via* 1,3 dipolar cycloaddition and amidation reaction, followed by further conjugation with radionuclide chelating moieties and biological antibodies or antibody fragments respectively. The resulting constructs possessed comparable degree of functionalization and were characterized thoroughly by means of many techniques such as TGA, TEM, gel electrophoresis and SPR. Successful and stable radiolabelling with ^{111}In was achieved, permitting the consequent *in vivo* biodistribution studies using γ-scintigraphy and SPECT imaging. Different organ biodistribution profiles over time were observed from these two *f*-MWNTs after *i.v.* injection, and the MWNTs with the higher aspect ratio displayed higher tissue affinity compared to the wider MWNTs. The results in this work demonstrate the impact of the diameter of CNTs that can influence their biological behaviours. The property of enhanced tissue distribution of the narrow MWNTs may be favourable for their potential biological applications as delivery carriers for diagnosis and therapy.

Acknowledgements

This work is supported by the European Union through ANTICARB (HEALTH-2007-201587), the University of Trieste, INSTM, the Italian Ministry of Education MIUR (Cofin Prot. 2010N3T9M4 and FIRB prot. RBAP11ETKA), and the CNRS. A.B. wishes to acknowledge the CNRS financial support from PICS (Project for International Scientific Cooperation). Partial support is also acknowledged by the Engineering and Physical Sciences Research Council research grant (grant EP/G061998/1) and CARBONANOBRIDGE (ERC-2008-AdG-227135) programs. TEM images were recorded at the RIO Microscopy Facility Platform of Esplanade Campus (Strasbourg, France). Authors would like to thank Mr Dan Asker, Institute of Pharmaceutical Science, King's College London for his technical help in the radioactivity experiments.

Appendix A. Supplementary data

Supplementary data related to this article can be found at http://dx.doi.org/10.1016/j.biomaterials.2014.07.054.

References

[1] Iijima S. Helical microtubules of graphitic carbon. Nature 1991;354:56–8.
[2] Martel R. Sorting carbon nanotubes for electronics. ACS Nano 2008;2:2195–9.
[3] Spitalsky Z, Tasis D, Papagelis K, Galiotis C. Carbon nanotube-polymer composites: chemistry, processing, mechanical and electrical properties. Prog Polym Sci 2010;35:357–401.
[4] Vashist SK, Zheng D, Al-Rubeaan K, Luong JHT, Sheu FS. Advances in carbon nanotube based electrochemical sensors for bioanalytical applications. Biotechnol Adv 2011;29:169–88.
[5] De Volder MFL, Tawfick SH, Baughman RH, Hart AJ. Carbon nanotubes: present and future commercial applications. Science 2013;339:535–9.
[6] Liu Z, Tabakman S, Welsher K, Dai HJ. Carbon nanotubes in biology and medicine: in vitro and in vivo detection, imaging and drug delivery. Nano Res 2009;2:85–120.
[7] Bianco A, Kostarelos K, Partidos CD, Prato M. Biomedical applications of functionalised carbon nanotubes. Chem Commun 2005:571–7.
[8] Kostarelos K, Bianco A, Prato M. Promises, facts and challenges for carbon nanotubes in imaging and therapeutics. Nat Nanotechnol 2009;4:627–33.
[9] Georgakilas V, Tagmatarchis N, Pantarotto D, Bianco A, Briand JP, Prato M. Amino acid functionalisation of water soluble carbon nanotubes. Chem Commun 2002:3050–1.
[10] Georgakilas V, Kordatos K, Prato M, Guldi DM, Holzinger M, Hirsch A. Organic functionalization of carbon nanotubes. J Am Chem Soc 2002;124:760–1.
[11] Ali-Boucetta H, Nunes A, Sainz R, Herrero MA, Tian B, Prato M, et al. Asbestos-like pathogenicity of long carbon nanotubes alleviated by chemical functionalization. Angew Chem Int Ed Engl 2013;52:2274–8.
[12] Dumortier H, Lacotte S, Pastorin G, Marega R, Wu W, Bonifazi D, et al. Functionalized carbon nanotubes are non-cytotoxic and preserve the functionality of primary immune cells. Nano Lett 2006;6:1522–8.
[13] Jain S, Thakare VS, Das M, Godugu C, Jain AK, Mathur R, et al. Toxicity of multiwalled carbon nanotubes with end defects critically depends on their functionalization density. Chem Res Toxicol 2011;24:2028–39.
[14] Lam CW, James JT, McCluskey R, Hunter RL. Pulmonary toxicity of single-wall carbon nanotubes in mice 7 and 90 days after intratracheal instillation. Toxicol Sci 2004;77:126–34.
[15] Liu Y, Zhao Y, Sun B, Chen C. Understanding the toxicity of carbon nanotubes. Acc Chem Res 2012;46:702–13.
[16] Schipper ML, Nakayama-Ratchford N, Davis CR, Kam NW, Chu P, Liu Z, et al. A pilot toxicology study of single-walled carbon nanotubes in a small sample of mice. Nat Nanotechnol 2008;3:216–21.
[17] Lacerda L, Herrero MA, Venner K, Bianco A, Prato M, Kostarelos K. Carbon-nanotube shape and individualization critical for renal excretion. Small 2008;4:1130–2.
[18] Kolosnjaj-Tabi J, Hartman KB, Boudjemaa S, Ananta JS, Morgant G, Szwarc H, et al. In vivo behavior of large doses of ultrashort and full-length single-walled carbon nanotubes after oral and intraperitoneal administration to Swiss mice. ACS Nano 2010;4:1481–92.
[19] Lacerda L, Ali-Boucetta H, Herrero MA, Pastorin G, Bianco A, Prato M, et al. Tissue histology and physiology following intravenous administration of different types of functionalized multiwalled carbon nanotubes. Nanomedicine (Lond) 2008;3:149–61.
[20] Bottini M, Rosato N, Bottini N. PEG-modified carbon nanotubes in biomedicine: current status and challenges ahead. Biomacromolecules 2011;12:3381–93.
[21] Liu Z, Cai W, He L, Nakayama N, Chen K, Sun X, et al. In vivo biodistribution and highly efficient tumour targeting of carbon nanotubes in mice. Nat Nanotechnol 2007;2:47–52.
[22] McDevitt MR, Chattopadhyay D, Kappel BJ, Jaggi JS, Schiffman SR, Antczak C, et al. Tumor targeting with antibody-functionalized, radiolabeled carbon nanotubes. J Nucl Med 2007;48:1180–9.
[23] Hong SY, Tobias G, Al-Jamal KT, Ballesteros B, Ali-Boucetta H, Lozano-Perez S, et al. Filled and glycosylated carbon nanotubes for in vivo radioemitter localization and imaging. Nat Mater 2010;9:485–90.
[24] Fenoglio I, Aldieri E, Gazzano E, Cesano F, Colonna M, Scarano D, et al. Thickness of multiwalled carbon nanotubes affects their lung toxicity. Chem Res Toxicol 2012;25:74–82.
[25] Yamashita K, Yoshioka Y, Higashisaka K, Morishita Y, Yoshida T, Fujimura M, et al. Carbon nanotubes elicit DNA damage and inflammatory response relative to their size and shape. Inflammation 2010;33:276–80.
[26] Pastorin G, Wu W, Wieckowski S, Briand JP, Kostarelos K, Prato M, et al. Double functionalisation of carbon nanotubes for multimodal drug delivery. Chem Commun 2006:1182–4.

[27] Riddles PW, Blakeley RL, Zerner B. Ellman's reagent: 5,5'-dithiobis(2-nitrobenzoic acid) – a reexamination. Anal Biochem 1979;94:75–81.
[28] Singh R, Pantarotto D, Lacerda L, Pastorin G, Klumpp C, Prato M, et al. Tissue biodistribution and blood clearance rates of intravenously administered carbon nanotube radiotracers. Proc Natl Acad Sci U S A 2006;103:3357–62.
[29] Jue R, Lambert JM, Pierce LR, Traut RR. Addition of sulfhydryl groups of *Escherichia coli* ribosomes by protein modification with 2-iminothiolane (methyl 4-mercaptobutyrimidate). Biochemistry 1978;17:5399–406.
[30] Venturelli E, Fabbro C, Chaloin O, Ménard-Moyon C, Smulski CR, Da Ros T, et al. Antibody covalent immobilization on carbon nanotubes and assessment of antigen binding. Small 2011;7:2179–87.
[31] Cooper MA. Optical biosensors in drug discovery. Nat Rev Drug Discov 2002;1:515–28.
[32] Karlsson R. SPR for molecular interaction analysis: a review of emerging application areas. J Mol Recognit 2004;17:151–61.
[33] Pantarotto D, Singh R, McCarthy D, Erhardt M, Briand JP, Prato M, et al. Functionalized carbon nanotubes for plasmid DNA gene delivery. Angew Chem Int Ed Engl 2004;43:5242–6.
[34] Al-Jamal KT, Nunes A, Methven L, Ali-Boucetta H, Li S, Toma FM, et al. Degree of chemical functionalization of carbon nanotubes determines tissue distribution and excretion profile. Angew Chem Int Ed Engl 2012;51:6389–93.
[35] Rooy I, Cakir-Tascioglu S, Hennink W, Storm G, Schiffelers R, Mastrobattista E. In vivo methods to study uptake of nanoparticles into the brain. Pharm Res 2011;28:456–71.
[36] Deen WM. What determines glomerular capillary permeability? J Clin Invest 2004;114:1412–4.
[37] McDevitt MR, Chattopadhyay D, Jaggi JS, Finn RD, Zanzonico PB, Villa C, et al. PET imaging of soluble yttrium-86-labeled carbon nanotubes in mice. PLoS One 2007;2:e907.
[38] Wang J, Deng XY, Yang ST, Wang HF, Zhao YL, Liu YF. Rapid translocation and pharmacokinetics of hydroxylated single-walled carbon nanotubes in mice. Nanotoxicology 2008;2:28–32.
[39] Lacerda L, Soundararajan A, Singh R, Pastorin G, Al-Jamal KT, Turton J, et al. Dynamic imaging of functionalized multi-walled carbon nanotube systemic circulation and urinary excretion. Adv Mater 2008;20:225–30.
[40] Deng X, Jia G, Wang H, Sun H, Wang X, Yang S, et al. Translocation and fate of multi-walled carbon nanotubes in vivo. Carbon 2007;45:1419–24.
[41] Yang ST, Guo W, Lin Y, Deng XY, Wang HF, Sun HF, et al. Biodistribution of pristine single-walled carbon nanotubes in vivo. J Phys Chem C 2007;111:17761–4.
[42] Ruggiero A, Villa CH, Holland JP, Sprinkle SR, May C, Lewis JS, et al. Imaging and treating tumor vasculature with targeted radiolabeled carbon nanotubes. Int J Nanomedicine 2010;5:783–802.